Angiotensin receptor conformations stabilized by biased ligands differentially modulate β-arrestin interactions

Matthias Elgeti[1,2*#], Julia Belyaeva[1*], Mahdi Bagherpoor Helabad[2,5], Dean P. Staus[3], Laura M. Wingler[4#]

[1]Institute for Drug Discovery and Institute for Medical Physics and Biophysics, University of Leipzig Medical School, Leipzig, Germany
[2]Integrative Center for Bioinformatics, University of Leipzig, Leipzig, Germany
[3]Department of Medicine, Duke University School of Medicine, Durham, NC, USA
[4]Department of Pharmacology and Cancer Biology, Duke University School of Medicine, Durham, NC, USA
[5]Current address: Institute of Chemistry, Martin-Luther-University Halle-Wittenberg, Halle (Saale), Germany
[6]Current address: Septerna, South San Francisco, CA, USA

*Equal authorship contribution
[#]To whom correspondence should be addressed: Matthias Elgeti (matthias.elgeti@uni-leipzig.de) or Laura M. Wingler (laura.wingler@duke.edu)

Abstract

"Biased" ligands of the angiotensin II type 1 receptor (AT1R) preferentially activate Gq pathways, which promote vasoconstriction, or β-arrestin-mediated pathways, which have salutary cardiac effects. We previously demonstrated that pharmacologically indistinguishable β-arrestin-biased ligands stabilize different AT1R conformational ensembles. Here we show these ligand-specific conformational changes determine whether β-arrestin interacts with the AT1R seven-transmembrane (7TM) core or only the phosphorylated C-terminus. We developed a method to form complexes between non-phosphorylated AT1R and β-arrestin1 mediated only through the 7TM core. β-Arrestin-biased ligands vary substantially in their ability to stabilize these complexes, with less effective ligands promoting intracellular conformations characterized by an intermediate rather than a fully outward-tilted position of transmembrane helix 6. Since certain β-arrestin functions are promoted by interactions with the GPCR 7TM core and others by interactions with phosphorylated regions, GPCR drugs could exploit this mechanism to achieve finer levels of bias and further diversify their therapeutic effects.

Introduction

Like most G protein-coupled receptors (GPCRs), the angiotensin II type 1 receptor (AT1R) activates multiple intracellular proteins upon binding of its endogenous agonist angiotensin II (AngII)[1,2]. First, AT1R activates heterotrimeric G proteins, principally Gq, initiating second messenger signaling cascades and other effects. In addition, GPCR kinase (GRK) phosphorylation of the AT1R C-terminus promotes β-arrestin binding. β-Arrestins have multiple functions, including scaffolding and allosterically activating kinases, acting as adapters for endocytic machinery, and sterically blocking heterotrimeric G protein binding, leading to desensitization. Importantly, Gq and β-arrestins have distinct cellular and physiological effects. While AT1R signaling through Gq culminates in vasoconstriction, AT1R activation of β-arrestins has anti-apoptotic and positive inotropic effects in the heart[3,4].

"Biased" ligands preferentially activate subsets of the cellular pathways downstream of GPCRs. The realization that GPCR ligands can exhibit this type of nuanced pharmacology has galvanized efforts to develop drugs that stimulate desired therapeutic effects but not on-target side effects. For example, β-arrestin-biased AT1R ligands, which activate β-arrestin-mediated but not Gq-mediated responses, have been investigated for acute heart failure[5,6] and acute respiratory distress syndrome associated with COVID-19[7,8].

An important reason GPCR ligands can show such complex pharmacology is that GPCRs are structurally heterogeneous proteins that sample multiple activated states. Agonist binding to the extracellular ligand-binding site ("orthosteric site") causes conformational changes that are propagated through the GPCR seven-transmembrane (7TM) helix bundle to the intracellular regions. We previously used double electron-electron resonance (DEER) to obtain a detailed picture of the conformational heterogeneity of the intracellular regions of AT1R[9]. This showed that different classes of AT1R ligands—antagonists, AngII, Gq-biased ligands, and β-arrestin-biased ligands—stabilize very different conformational distributions. Unexpectedly, we also observed that ligands within the same pharmacological class, specifically β-arrestin-biased ligands, can give rise to different conformational distributions. We refer to a ligand's propensity to stabilize specific intracellular conformations as its "conformational efficacy[10]."

β-Arrestins are also conformationally heterogeneous proteins, and they can engage GPCRs through multiple binding modes[11,12]. β-Arrestins can interact with GPCRs through GRK-phosphorylated regions in the C-terminus or intracellular loop 3 (ICL3) ("phosphosite interaction") and/or through the GPCR 7TM core, the same region to which G proteins bind[11,13]. Besides these two principal interfaces, β-arrestins have also been observed to interact with the cytosolic Helix 8 (H8) of the glucagon receptor[14] and with membrane lipids[14-17]. Since β-arrestins typically have higher affinity for the phosphosite than for the 7TM core, GPCR/β-arrestin complexes equilibrate between conformations where β-arrestin is engaged with one or both sites[18]. This equilibrium has important implications because each interaction is associated with different functions of β-arrestins. While the phosphosite interaction is sufficient to promote GPCR internalization and initiate β-arrestin-dependent signaling, the 7TM core interaction is required for β-arrestins to sterically block G protein activation[19,20].

The distinct intracellular conformations stabilized by orthosteric AT1R ligands could directly regulate the interaction of β-arrestins with the 7TM core. However, ligand effects on the 7TM core interaction have been difficult to evaluate, as most conventional readouts of β-arrestin activation reflect the phosphosite interaction. Accordingly, we developed an *in vitro* method to form AT1R/β-arrestin complexes mediated only by the 7TM core. We find that β-arrestin-biased ligands vary in their ability to stabilize such complexes, and this variation correlates with ligands' conformational efficacy. DEER and MD simulation data provide a mechanistic explanation for why β-arrestin cannot robustly interact with one of the conformations stabilized by β-arrestin-

biased ligands. These findings suggest that orthosteric ligands could bias the functions of β-arrestins by allosterically regulating the conformational equilibrium of GPCR/β-arrestin complexes.

Results

β-arrestin1 interacts with the AT1R 7TM core in a ligand-dependent manner

We developed a strategy to investigate the interaction of β-arrestin with the AT1R 7TM core. To activate β-arrestin, we purified a complex of β-arrestin1, a synthetic phosphopeptide from the C-terminus of the V2 vasopressin receptor (V2R), and conformationally selective antibody fragments[15,21,22] **(Figure 1A)**. These binding partners effectively promote conformational changes in β-arrestin1 that facilitate its interaction with the 7TM core of GPCRs, including interdomain rotation and stabilization of the extended finger loop[21]. Competition radioligand binding confirms that the activated β-arrestin1 complex (βarr1*) allosterically increases the affinity of AngII but not the antagonist losartan for purified, non-phosphorylated AT1R in an MNG micellar environment **(Figure 1B,C; Supplementary Table 1)**. By size exclusion chromatography (SEC), AngII-bound AT1R co-migrates with βarr1*, as evidenced by a reduced retention time **(Figure 1D)**. In contrast, complexes formed with the high-affinity antagonist candesartan dissociate. These data demonstrate that AT1R and βarr1* productively interact in an agonist-dependent manner through the receptor's 7TM core.

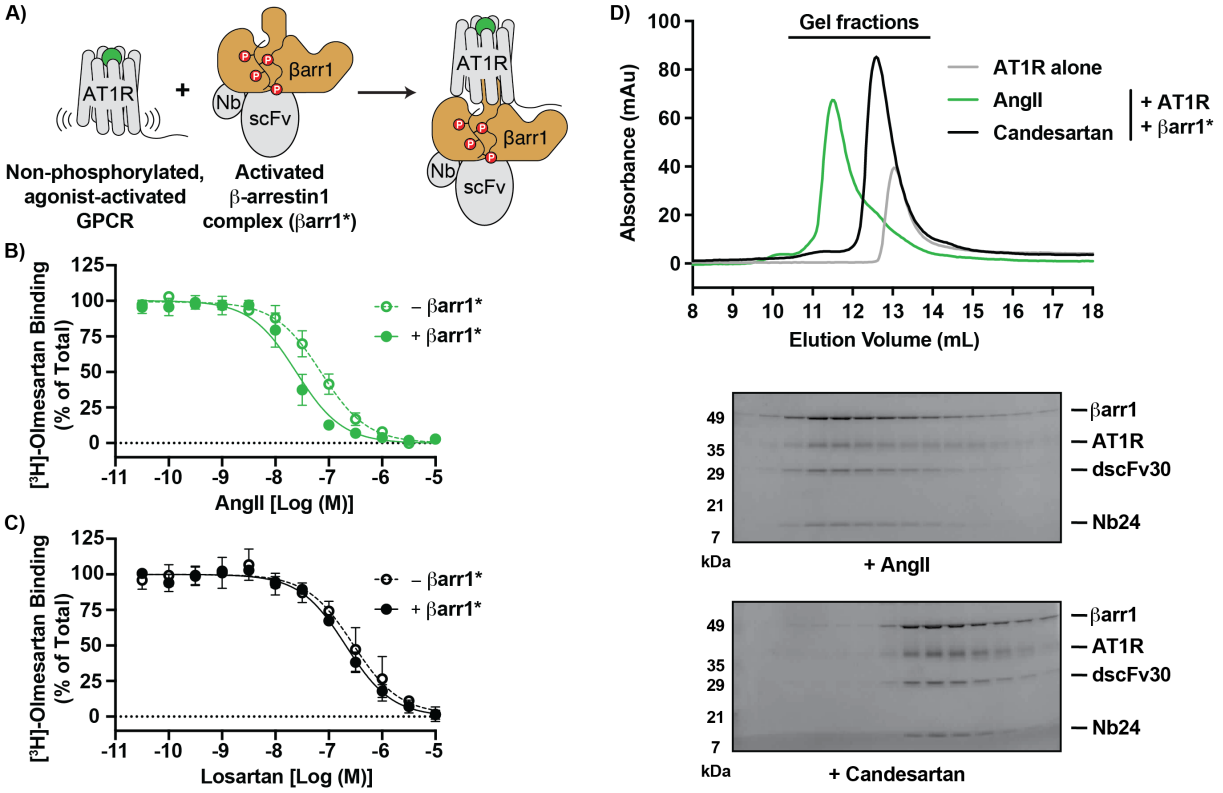

Figure 1. Formation of 7TM core-mediated AT1R/β-arrestin complexes. (A) *Schematic of complex formation strategy. Purified, non-phosphorylated AT1R bound to various orthosteric ligands is incubated with βarr1*, a purified complex of β-arrestin1, the synthetic V2R phosphopeptide (V2Rpp), and the active-state-specific β-arrestin1 binders dscFv30 (or Fab30) and Nb24.* ***(B,C)*** *Competition binding between the radiolabeled antagonist [^{3}H]-olmesartan and unlabeled (B) AngII or (C) losartan at purified AT1R in the absence or presence of βarr1* (2.5 μM). Log IC_{50} values are provided in* ***Supplementary Table 1****. Data represent the mean ± S.D. of 3 independent experiments.* ***(D)*** *SEC and gel electrophoresis analysis*

(Coomassie staining) of deglycosylated AT1R/βarr1 complexes formed in the presence of AngII or candesartan.*

Intracellular conformation of βarr1-bound AT1R*

To analyze the intracellular conformational ensemble of AT1R, we previously established ten spin label pairs that cover the cytoplasmic receptor surface[9], including sites in TM1, TM5, TM6, TM7, ICL2, and H8 **(Figure 2A)**. We acquired DEER data for each of these pairs in the presence of excess AngII and βarr1*. Due to the technical challenges associated with forming stable AT1R-Gq complexes *in vitro*[23], for comparison we also collected DEER measurements in the presence of AngII and AT110i1. AT110i1 is a conformationally selective nanobody (Nb, single-domain antibody fragment) that binds to the intracellular transducer pocket, which we previously used to crystallize AT1R in an activated state[24].

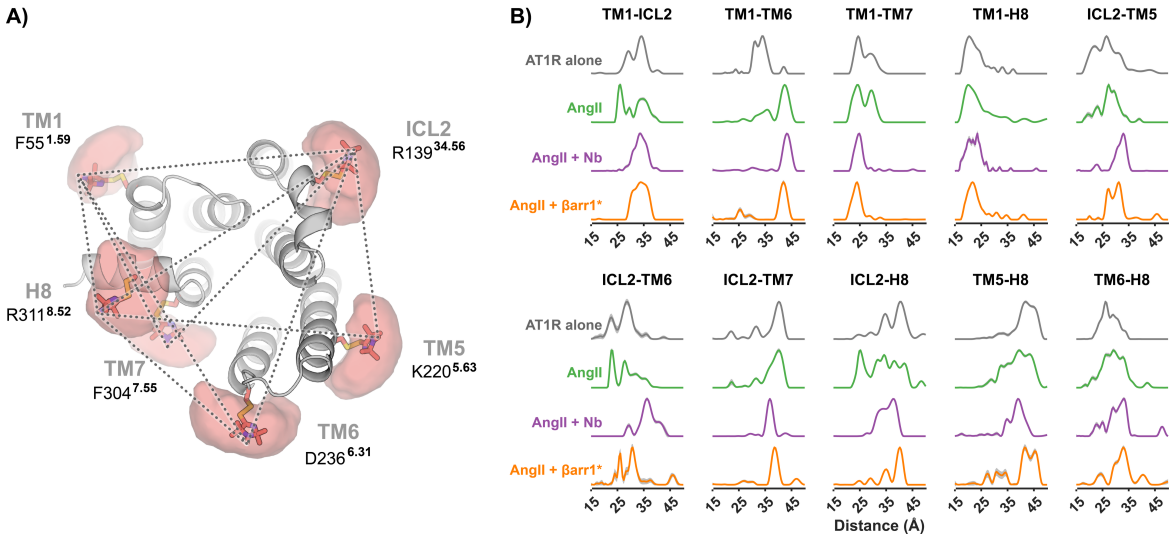

Figure 2. DEER analysis of AT1R bound to different intracellular binding partners. A) *Spin label positions and pairwise combinations (dashed lines) used to record distances in this study. Spin labels are shown as sticks; clouds indicate the possible positions of the unpaired electron.* ***B)*** *Probability distance distributions between the indicated spin pairs showing the effects of AngII (green), AngII + Nb AT110i1 (purple), and AngII + βarr1* (orange) on apo AT1R (gray). Shaded areas indicate 95% confidence intervals. Associated raw DEER data and dipolar analyses are shown in* ***Supplementary Figure 1****.*

As previously reported[9], AngII populates a heterogeneous ensemble of conformations, some of which exhibit characteristics of GPCR activation **(Figure 2B)**. These include the outward displacement of TM6 (cf. TM1-TM6 distances) and the inward movement of TM7 (cf. ICL2-TM7 distances). Addition of either βarr1* or Nb AT110i1 markedly reduces this conformational heterogeneity **(Figure 2B)**. Both proteins stabilize an active conformational state of TM6 (TM1-TM6 ~42 Å). In the presence of βarr1*, a peak at 24 Å also appears, which could correspond to an active state with a rotated position of TM6, as previously observed for rhodopsin-transducin complexes[25]. Most pairs involving the ICL2 and H8 labeling sites show two major populations in the presence of βarr1*, indicating that flexibility remains in these regions. AT110i1 stabilizes an even less heterogeneous conformational ensemble than βarr1*, with a notable stabilization of ICL2. We conclude that both intracellular binding partners bind AT1R in a similar binding mode involving an outward-tilted TM6, but they differ in their interaction with other parts of the intracellular receptor surface, such as ICL2 and TM5.

β-arrestin-biased ligands differentially stabilize AT1R/βarr1 complexes*

TRV023, TRV026, and TRV027 are well-characterized biased ligands that recruit β-arrestin to the plasma membrane with almost indistinguishable potencies and efficacies **(Figure 3A)**, consistent with previously reported data[26,27]. Even though their pharmacological profiles are similar, our previous DEER data showed these β-arrestin-biased ligands stabilize intracellular conformational distributions that are not only different from other ligand classes but also different from each other[9] **(Supplementary Figure 2)**. In the main conformation stabilized by TRV026, designated "Occluded 1," TM6 moves to an intermediate rather than the fully outward position (TM1-TM6 35 Å), but the conformation does exhibit a characteristic inward movement of TM7 (cf. ICL2-TM7 distances) and a substantial movement of H8 (cf. ICL2-H8 and TM5-H8 distances). In the main conformation stabilized by TRV023, designated "Occluded 2," TM6 moves to the fully outward position (TM1-TM6 42 Å). However, mapping of the characteristic peaks indicates that TM5 does not rotate to the same extent as the fully activated conformation stabilized by AngII and Gq-biased ligands, and ICL2 undergoes a major conformational change[9]. TRV027 stabilizes approximately equal populations of Occluded 1 and Occluded 2[9].

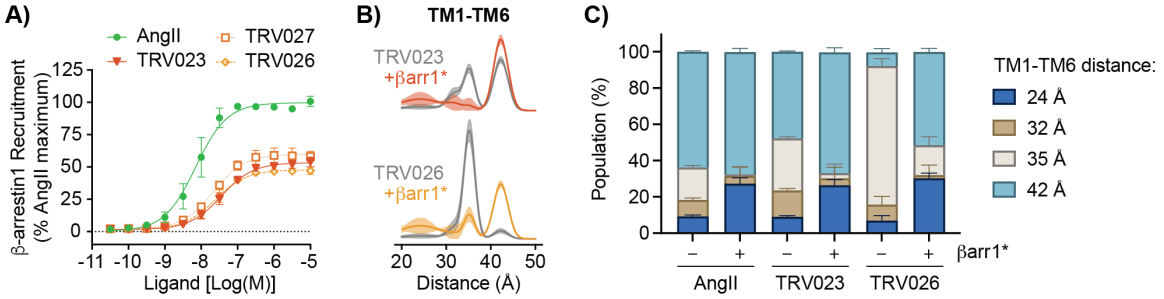

Figure 3. Formation of AT1R/βarr1* complexes by β-arrestin-biased ligands. A) *Ligand-induced β-arrestin1 recruitment to the cell plasma membrane. Data are normalized to the AngII maximum response and represent the mean ± S.D. of 3 independent experiments. Curve analysis parameters are provided in* ***Supplementary Table 2****.* ***B)*** *TM1-TM6 probability distance distributions for biased ligands TRV023 and TRV026 in the absence (gray) and presence (colored) of βarr1*. Shaded areas indicate 95% confidence intervals. The associated raw DEER data and model-based analysis are shown in* ***Supplementary Figure 1****.* ***C)*** *Median populations ± 95% confidence intervals of Gaussian populations centered around 24, 32, 35, and 42 Å for TM1-TM6 distance distributions. Populations are provided in* ***Supplementary Table 3****.*

We asked whether there would be differences among AT1R/βarr1* complexes formed in the presence of these β-arrestin-biased ligands. We performed DEER measurements on our TM1-TM6 pair bound to TRV023 and TRV026 in the absence and presence of βarr1* **(Figure 3B)**. The addition of βarr1* quantitatively stabilizes the same 24 Å and 42 Å distances for both AngII and TRV023 **(Figure 2B, 3B, 3C)**. However, even though DEER experiments are performed at mid-micromolar protein concentrations, βarr1* does not fully deplete the 35 Å population in the presence of TRV026. The incomplete complex formation observed even at high protein concentrations suggests that βarr1* has substantially lower affinity for TRV026-AT1R than for AngII-AT1R and TRV023-AT1R.

To quantitatively assess the ligand dependence of complex affinity, we employed an AlphaScreen proximity assay that allows us to detect the interaction between FLAG-AT1R and βarr1* (through a His6-tagged antibody fragment) at mid-nanomolar protein concentrations. While TRV023 is at least as effective as AngII in promoting βarr1* complex formation, TRV026 does not give an appreciable signal in this assay **(Figure 4A)**. Importantly, the difference in βarr1* interaction is not due to lower ligand affinity, since the affinity of TRV026 for purified AT1R is comparable to AngII and higher than TRV023[26]. In addition, TRV055, a much lower affinity agonist that stabilizes fully activated AT1R conformations[9], effectively promotes complex formation.

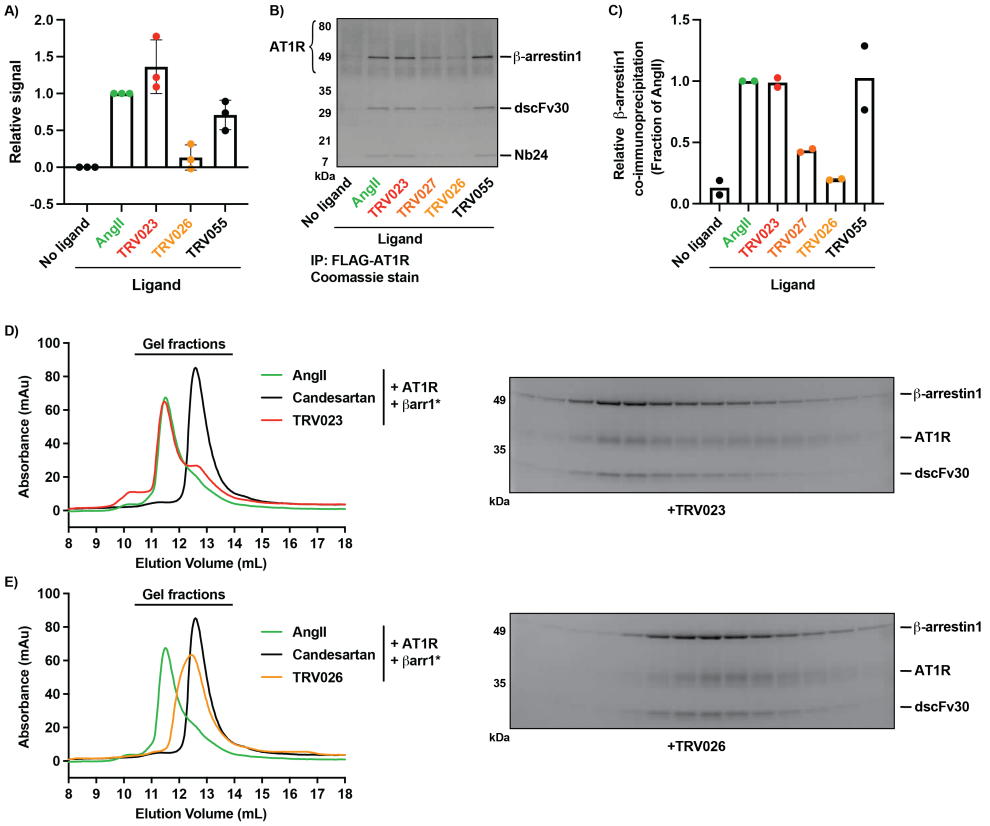

Figure 4. Ligand-dependent stability of AT1R/βarr1* complexes. (A) *AlphaScreen assay detecting the interaction between FLAG-tagged AT1R (100 nM) and βarr1* (33 nM) (via His6-tagged Fab30) in the presence of saturating concentrations of various ligands. Data are normalized to the no ligand/AngII signals and represent the mean ± S.D. of 3 independent experiments.* ***(B, C)*** *Co-immunoprecipitation of βarr1* with AT1R (glycosylated) in the presence of saturating concentrations of various ligands. (B) shows a representative Coomassie-stained gel; (C) shows quantitation of the β-arrestin1 band from 2 independent experiments.* ***(D,E)*** *Stability of deglycosylated AT1R/βarr1* complexes formed with (D) TRV023 and (E) TRV026 as assessed by SEC and gel electrophoresis of the resulting fractions.*

We further asked how various β-arrestin-biased ligands affect the rate of dissociation of AT1R/βarr1* complexes using co-immunoprecipitation. Here complexes are formed at micromolar concentrations, but βarr1* can dissociate during washing. TRV055 and TRV023 promote βarr1* pulldown as effectively as AngII **(Figure 4B,C)**. TRV027 and TRV026 are increasingly less effective.

Finally, we analyzed the ability of biased ligands to stabilize AT1R/βarr1* complexes by SEC. TRV023 complexes remain mostly intact, with the majority eluting at the shorter retention time observed for AngII **(Figure 4D)**. In contrast, TRV026 complexes largely dissociate, with a broad peak migrating closer to the retention time of candesartan-bound AT1R **(Figure 4E)**. Together these data demonstrate that βarr1* has lower affinity for the AT1R 7TM core in the presence of TRV026 compared to TRV023 and AngII.

TRV026-stabilized conformations observed in silico do not accommodate β-arrestin binding to the 7TM core

DEER shows that TRV026 stabilizes a structural intermediate that we previously designated Occluded 1[9], and our functional data indicate βarr1* cannot effectively engage this conformation through the 7TM core. We used unbiased molecular dynamics (MD) simulations to obtain an all-

atom structural model of the TRV026-bound conformation. We performed five MD replicas of 20 μs each to capture conformational transitions between different TM6 conformations that occur on a slow timescale[28]. Simulations were initiated from an inactive conformation of AT1R[29] (PDB ID: 4YAY), a choice which was motivated by previously reported challenges in capturing large conformational changes in MD simulations initiated from active AT1R[30]. To compare our MD simulations with the experimental DEER distance distributions, we attached spin labels *in silico* to all experimental labeling sites and simulated the corresponding distance distributions for each MD frame (see Materials and Methods). In three out of five replicas, TM6 moved outward by about 2 Å, similar to the distance change observed in DEER[9] (TM1-TM6 distance 32 Å for inactive conformation vs. 35 Å for Occluded 1) **(Supplementary Figure 2)**.

In one replica, TM6 transitioned after the first 5 μs and stably maintained the intermediate position until the end of the simulation **(Figure 5A)**. The time evolution of simulated peak positions for all ten spin label pairs in this replica are shown in **Supplementary Figure 3**. To determine a representative structure of the intermediate conformation, we calculated the median structure of all MD simulation frames after the first 5 μs **(Figure 5A)**. This structural model confirms that TM6 assumes an intermediate position relative to inactive- and active-state AT1R structures **(Figure 5B)**. Another prominent change is that H8 moves to a membrane-normal orientation. This position of H8 is distinct both from inactive AT1R structures, where it is angled slightly away from the membrane[29], and from active AT1R structures, where it lies parallel to the membrane[24], as is typical for most GPCRs. A similar membrane-normal position of H8 has been observed for other GPCRs[31]. Unlike many GPCRs, AT1R lacks a palmitoylation site in H8, which likely increases structural flexibility in this segment. Notably, our previous DEER data indicated conformational changes in the TRV026-stabilized Occluded 1 conformation that are consistent with the out-of-plane movement of H8[9].

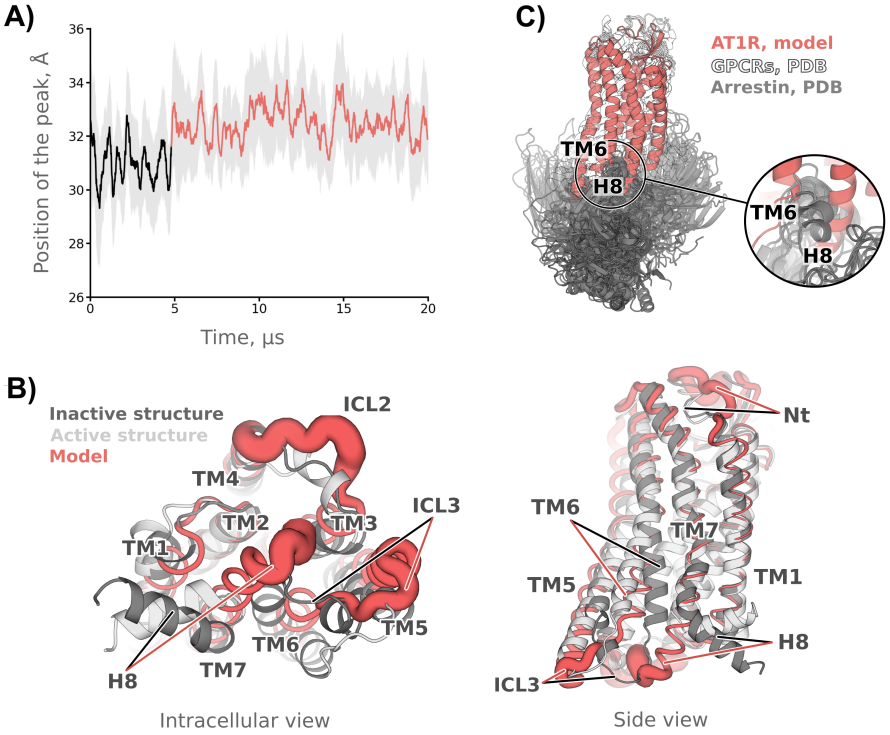

Figure 5. MD analysis of AT1R bound to TRV026. (A) *Peak distance of the modeled TM1-TM6 distance distribution over simulation time. The bold line represents the sliding mean, and the semi-transparent gray area indicates the standard deviation. After about 5 μs, the inactive-like peak position (black line) shifts toward an intermediate distance (red line).* ***(B)*** *Intracellular and side views of the AT1R structural model*

with the intermediate TM6 position (red). The active (light gray, PDB: 6OS2) and inactive (dark gray, PDB: 4YAY) AT1R structures are shown for comparison. Backbone flexibility is visualized by mapping the RMSF to the width of the cartoon representation. ***(C)*** *Superposition of GPCR–arrestin core complexes with the model of the TRV026-bound intermediate conformation. All observed poses of visual arrestin and β-arrestin1 clash with TM6 and H8 of the AT1R model.*

We also evaluated the flexibility of individual protein segments by calculating the backbone root mean square fluctuation (RMSF) values **(Figure 5B)**. The N-terminus, ICL2 and H8 show the highest flexibility in the intermediate conformation, which may have functional relevance for those segments. ICL3 was less dynamic than those regions, and the 7TM region remained largely stable.

Finally, we asked whether the 7TM core of this TRV026-stabilized AT1R conformation could engage β-arrestins. To this end, we superimposed all available core-engaged, high-resolution structures of GPCRs in complex with β-arrestin1 or visual arrestin on the intermediate model described above **(Figure 5C)**. Both TM6 and H8 of the intermediate model clash with arrestins, particularly with the finger loop that inserts into the GPCR transducer-binding pocket. This accords with our DEER data showing that driving complex formation between TRV026-bound AT1R and βarr1* at high protein concentrations leads to the outward displacement of TM6 **(Figure 3B)**.

Discussion

The multimodal interactions of β-arrestins with GPCRs results in several types of conformational heterogeneity within the resulting complexes[15,18,32]. First, complexes can sample conformations where β-arrestin is bound only to the phosphosite and where β-arrestin is bound both to the phosphosite and the 7TM core[15,18]. Second, complexes can retain substantial plasticity even when β-arrestin interacts with the 7TM core. In this manuscript, we have developed methodology to form AT1R/β-arrestin complexes mediated exclusively by interactions through the 7TM core of AT1R, providing insights into both of these aspects of conformational heterogeneity. Our *in vitro* analysis of AT1R/β-arrestin complexes is limited by the detergent environment of the receptor[25,33] and by the use of the same phosphorylated peptide and antibody fragments to stabilize an activated conformation of β-arrestin1. Interactions with membrane lipids[14-17,34,35] and alternative phosphorylation patterns[36,37] could influence the conformational distribution of β-arrestin and its interaction with the AT1R 7TM core. Nevertheless, our findings suggest a potentially important mechanism through which ligands could bias the activation of different β-arrestin-mediated pathways.

Numerous biophysical approaches have revealed conformational heterogeneity in complexes where β-arrestin is fully engaged with the GPCR 7TM core. High-resolution cryo-electron microscopy structures show that β-arrestin can assume many orientations relative to the 7TM core of various GPCRs[15,16,32,38-41]. Intermolecular DEER measurements of rhodopsin/visual arrestin observed multiple distances, indicative of flexibility within the complex[42]. NMR studies of GPCRs bound to mutationally activated β-arrestin1 have highlighted the dynamics of residues throughout the receptors, from the ligand-binding site to the intracellular face[43,44]. Consistent with these studies, our DEER data show conformational heterogeneity in certain intracellular regions of the AT1R, particularly H8, when bound to βarr1* **(Figure 2B)**. On the other hand, several intracellular receptor segments, such as TM6, TM7 and ICL2, are stabilized by βarr1*. Furthermore, the βarr1*-complexed AT1R conformation shows subtle but defined structural differences compared to AT1R bound to an active state-specific Nb and presumably also to heterotrimeric Gq.

277 AngII, TRV023, and TRV026 each stabilize distinct AT1R conformational distributions in the
278 absence of transducers[9]. Yet to the extent that our DEER probes can resolve, the same
279 intracellular conformation dominates in the presence of high concentrations of βarr1*, regardless
280 of which ligand is bound **(Figure 3B)**. This is not surprising since the intracellular AT1R
281 conformation in the final complex will be largely dictated by the direct interactions this region
282 makes with the transducer[26,45]. In contrast, the addition of β-arrestin1 to phosphorylated μ-opioid
283 receptor (μOR) bound to full, partial, or biased agonists had minimal effects on the μOR
284 intracellular conformational distribution by DEER. The difference between the AT1R and μOR
285 systems may be due to the relatively low affinity of β-arrestin1 for the μOR 7TM core. We
286 previously demonstrated that μOR/β-arrestin1 complexes are predominantly in conformations
287 where β-arrestin1 only engages the phosphosite[46].

288 Despite the similarity of the dominant AT1R conformation in βarr1* complexes formed with various
289 orthosteric ligands, we found that βarr1* has a lower affinity for and dissociates more quickly from
290 AT1R bound to TRV026 **(Figure 4)**. TRV026 stabilizes the Occluded 1 conformation that is
291 characterized by an intermediate position of TM6. Ligands that stabilize conformations with a
292 fully displaced TM6 promote more stable complex formation. This includes both TRV023, which
293 stabilizes the Occluded 2 conformation, and ligands such as AngII and TRV055, which stabilize
294 the canonical, fully activated conformation[9]. This indicates that even though the Occluded 1 and
295 Occluded 2 conformations are both stabilized by β-arrestin-biased AT1R ligands, they have
296 different efficacies towards βarr1* engagement of the core. Previous data have shown that
297 TRV027 only promotes interactions of β-arrestins with the phosphorylated C-terminus of AT1R,
298 while AngII stabilizes complexes with both phosphosite and 7TM core engagement[47]. This was
299 hypothesized to be due to GRK subtype-specific phosphorylation promoted by these ligands[47,48].
300 Our data suggest that the allosteric effects of orthosteric ligands on the core could also directly
301 influence the position of the equilibrium between "phosphosite only" and "phosphosite + core"
302 conformations.

303 Even though TRV026, TRV027, and TRV023 differ in their ability to stabilize the 7TM core
304 interaction with β-arrestins, they have similar efficacies and potencies in assays of β-arrestin
305 recruitment, internalization, and kinase pathway activation[26,27] **(Figure 3A)**. All these functional
306 responses can be mediated by β-arrestins when they are restricted to "phosphosite only"
307 conformations, in the absence of 7TM core engagement[19]. Therefore, these assays likely reflect
308 the comparable ability of these β-arrestin-biased ligands to promote GRK phosphorylation of the
309 C-terminus, the main driver of β-arrestin recruitment to the AT1R[47,49]. Other responses mediated
310 by β-arrestins, such as desensitization of G protein activation by steric blockade, are known to
311 correlate with the strength of the 7TM core interaction[19,46]. In some systems, the core interaction
312 has also been shown to modulate ERK activation[50]. Altering the equilibrium between the
313 "phosphosite" and "phosphosite + core" conformations thus provides a potential mechanism to
314 bias the manifold functions of β-arrestins. Notably, comparisons of several β-arrestin-biased
315 AT1R ligands in both proximal assays of β-arrestin activation and downstream signaling have
316 provided evidence of bias within this pharmacological class[51,52].

317 Our MD simulations provide a molecular rationale for the inability of βarr1* to engage the 7TM
318 core of TRV026-bound AT1R effectively **(Figure 5)**, despite the structural plasticity of arrestins.
319 Conversely, the increased dynamics of H8 observed by both DEER[9] **(Supplementary Figure 2)**
320 and in simulation **(Figure 5B)** upon TRV026 binding could facilitate the exposure of C-terminal
321 sites for phosphorylation by GRKs. The ligand dependence of β-arrestin interactions with the
322 7TM core may vary among GPCRs. NMR studies indicate that β-arrestin1 in complex with a
323 phosphorylated β2-adrenergic receptor (β2AR)/V2R chimera undergoes ligand-dependent
324 conformational changes that do not consistently correlate with ligands' efficacy towards G protein
325 activation or β-arrestin-dependent internalization[53]. This suggests that β-arrestin is sensitive to

326 the conformation of the β2AR core, as we have shown here for AT1R. In contrast, purified
327 β1-adrenergic receptor forms 7TM-core-mediated complexes with V2Rpp-activated β-arrestin1
328 equally well regardless of whether no ligand, an antagonist, an agonist, or a β-arrestin-biased
329 ligand is bound[54].

330 In summary, our data show that the conformational efficacy of β-arrestin-biased AT1R ligands
331 correlates with their ability to promote β-arrestin interactions with the AT1R 7TM core. There are
332 now several examples of functionally similar ligands that activate the same GPCR through distinct
333 mechanisms, including M2 muscarinic receptor partial agonists[55] and β2AR partial agonists[56].
334 This raises the possibility that there may be finer levels of ligand bias—and additional
335 opportunities to tune the pharmacology of GPCR drugs—that would not be detected in standard
336 high-throughput screening assays. Most β-arrestin activation assays monitor its recruitment to
337 GPCRs, principally reflecting β-arrestin's high-affinity interaction with GRK-phosphorylated
338 regions. On the other hand, efforts to rationally design β-arrestin-biased ligands have been based
339 on 7TM core-engaged GPCR/β-arrestin structures. Our findings suggest that these interactions
340 may not always be correlated. To maximize the likelihood of developing GPCR drugs with the
341 desired pharmacological profiles, it will be important to determine how different modes of
342 β-arrestin interactions influence the cellular responses of interest and to tailor drug discovery
343 approaches accordingly.

Methods

Cell lines. Expi293F Inducible cells (Thermo) were grown in Expi293 expression media (Thermo) with shaking at 110 rpm in a humidified 37 °C incubator with 8% CO_2.

Protein expression and purification. FLAG-tagged AT1R constructs were expressed in Expi293F Inducible cells transiently transfected with the Expifectamine transfection kit (Thermo) as previously described[9,24], and expression was induced two days after transfection with 4 μg/mL doxycycline and 5 mM sodium butyrate in the presence of 1 um losartan, a low-affinity antagonist. Cells were harvested approximately 30 hours after induction, washed with phosphate-buffered saline and 1 μM losartan, and flash frozen. Cells were lysed under hypotonic conditions (10 mM Tris pH 7.4, 2 mM EDTA, 10 mM $MgCl_2$, 1 μM losartan, 2.5 U/mL benzonase (Sigma), protease inhibitors benzamidine and leupeptin) and then dounced and solubilized for 2 hours at 4 °C (0.5% lauryl maltose neopentyl glycol (MNG), 0.05% cholesterol hemisuccinate (CHS), 20 mM HEPES pH 7.4, 500 mM NaCl, 10 mM $MgCl_2$, 1 μM losartan, benzonase, benzamidine, leupeptin). After centrifugation (30,000 × g, 30 min, 4 °C), 2 mM $CaCl_2$ was added, and solubilized material was loaded onto M1 anti-FLAG resin at 4 °C. The resin was washed (20 mM HEPES pH 7.4, 500 mM NaCl, 0.01% MNG, 0.01% CHS, 2 mM $CaCl_2$, benzamidine, leupeptin) and eluted (20 mM HEPES pH 7.4, 500 mM NaCl, 0.01% MNG, 0.01% CHS, 0.2 mg/mL FLAG-peptide). The protein was subjected to size exclusion chromatography (SEC) (Superdex 200 Increase 10/300 GL column, GE) in buffer consisting of 20 mM HEPES pH 7.4, 100 mM NaCl, 0.01% MNG, 0.001% CHS, and monomeric fractions were concentrated.

For DEER experiments, AT1R was eluted from M1 resin using buffer at pH 6.8 and incubated with a 20-fold molar excess of bis-(2,2,5,5-tetramethyl-3-imidazoline-1-oxyl-4-yl)disulfide (Enzo) for 3 hours at room temperature. SEC buffer was made with D_2O and contained 40 mM HEPES. For analytical SEC experiments, transfected cells were cultured in the presence of 5 uM kifunensine, and purified receptor was deglycosylated with EndoH for 90 minutes at room temperature before SEC[24].

Cysteine-free rat β-arrestin1 truncated at residue 393 was purified as a thrombin-cleavable GST fusion from BL21 DE3 *E. coli* as previously described[46]. Briefly, cells were lysed with a microfluidizer, and the fusion was captured on glutathione sepharose resin. After thrombin digest, β-arrestin1 was isolated by ion exchange chromatography (HiTrap Q sepharose). His-tagged antibody fragments that recognize an activated conformation of β-arrestin1 were purified as follows. Fab30 was purified as described previously[21]. A disulfide-stabilized single chain version of Fab30[15] (dscFv30) and the nanobody Nb24[15] were expressed in T7 Express lysY BL21 *E. coli* (New England Biolabs) and purified from the periplasmic fraction via NiNTA chromatography as previously described[24]; dscFv30 was expressed as a 3C-protease cleavable maltose-binding protein (MBP) fusion. To form the βarr1* complex, β-arrestin1 was incubated overnight at 4 °C with a 1.25 molar excess of V2Rpp phosphopeptide (ARGRpTPPpSLGPQDEpSCpTpTApSpSpSLAKDTSS), MBP-dscFv30, and Nb24. The complex was treated with 3C protease for 90 minutes at room temperature and purified by SEC (Superdex 200 Increase 10/300 GL column) in 20 mM HEPES pH 7.4, 100 mM NaCl. For DEER experiments, SEC buffer was made with D_2O.

DEER experiments. DEER samples consisted of spin-labeled AT1R (110 μM), βarr1* (140 μM), 1 mM ligand, and 20% d^8-glycerol (Cambridge Isotopes) in a final volume of 12 μL. After a 1 hour incubation at room temperature, binding reactions were transferred to in 1.4/1.7 mm (i.d./o.d.) borosilicate capillaries (VitroCom, Mountain Lakes, NJ), flash frozen, and stored at -80 °C.

394 4-Pulse DEER experiments were conducted at 50 K on a Q-band upgraded ElexSys 580 (Bruker,
395 Germany) equipped with an arbitrary waveform generator, a 150 W traveling wave tube amplifier
396 and a QT-2 probehead (Bruker) using the standard dead time free sequence[57]. Pulse lengths
397 were optimized using echo nutation experiments and set to 16-20 ns and 32-40 ns for pi/2 and pi-
398 pulses, respectively. A 100 ns 50 MHz-chirp pulse was applied as a pump pulse 70 MHz above
399 the observer frequency.
400
401 *DEER data analysis.* Dipolar evolutions were recorded with 16 ns time resolution and analyzed
402 model-free in LongDistances v.1112[58]. The smoothness parameter was determined by L-curve
403 criterion. Standard deviations for distances were determined using the error analysis
404 implementation in LongDistances using standard parameters and the inherited model-free
405 parameters. Population analysis was performed using a global Gaussian mixture model
406 implemented in the DeerLab Python toolbox. Positions and widths of the Gaussians were treated
407 as global fitting parameters, while populations, concentrations and modulation depths were local
408 parameters. 95% confidence bands were estimated via bootstrapping (100 iterations).
409
410 *Radioligand binding.* Purified AT1R (75 ng) was incubated with βarr1* (2.5 μM), [3H]-olmesartan
411 (American Radiolabeled Chemicals) and varying concentrations of cold competitor ligand in assay
412 buffer (20 mM HEPES pH 7.4, 100 mM NaCl, 0.01% MNG, 0.001% CHS, 0.1% BSA) in a total
413 volume of 200 μL for 2 hours at room temperature. Binding reactions were harvested onto GF/B
414 filters using a 96-well Brandel harvester and washed with cold 20 mM HEPES, 100 mM NaCl.
415 Bound radioactivity was measured using a Packard TriCarb 2100TR scintillation counter, and a
416 3-parameter dose-response curve was fit to the normalized data from 3 independent experiments
417 (GraphPad Prism).
418
419 *Analytical SEC*. Deglycosylated AT1R (12 μM) was incubated with ligand (333 μM) for 15 minutes
420 at room temperature, and β-arrestin1* (12 μM) was added for a total volume of 100 μL. After an
421 additional 1 hour incubation at room temperature, samples were loaded onto SEC (Superdex 200
422 Increase 10/300 GL column, 0.5 mL/min flow rate, 0.25 mL fractions). Fractions were analyzed
423 by gel electrophoresis.
424
425 *Co-immunoprecipitation*. Purified AT1R (7 μM) was incubated for 1 hour at room temperature
426 with ligand (1 mM) and βarr1* (9 μM) in assay buffer (20 mM HEPES pH 7.4, 100 mM NaCl,
427 0.001% MNG, 0.0001% CHS). Additional assay buffer (30 μL), $CaCl_2$ (2 mM) and M1 anti-FLAG
428 resin (20 μL) were added, and samples were rotated for 20 minutes at room temperature. The
429 resin was washed 4 times with assay buffer containing 2 mM $CaCl_2$ and then eluted with assay
430 buffer containing 5 mM EDTA and FLAG peptide. Eluates were analyzed by gel electrophoresis,
431 and bands were quantified in ImageJ.
432
433 *AlphaScreen*. βArr1* complex was formed *in situ* by incubating His-tagged Fab30 (17 μM) with a
434 2-fold excess of β-arrestin1 and V2Rpp for 1 hour at room temperature and then diluting 250-fold
435 in 20 mM HEPES pH 7.4, 100 mM NaCl, 0.1% BSA for a working Fab30 concentration of 67 nM.
436 Purified AT1R (200 nM) was incubated with ligand (200 μM) for 15 minutes at room temperature
437 in 20 mM HEPES pH 7.4, 100 mM NaCl, 0.01% MNG/0.001% CHS, 0.1% BSA. βarr1* (10 μL)
438 and ligand-bound AT1R (10 μL) were combined and incubated for 1 hour before the simultaneous
439 addition of anti-FLAG-conjugated AlphaScreen Acceptor beads (0.05 mg/well) and Nickel Chelate
440 Alpha Donor beads (0.05 mg/well) (Perkin Elmer) in a 5 μL volume. The signal resulting from the
441 close proximity of FLAG-AT1R and Fab30-His6 was read on a CLARIOstar plate reader (BMG
442 Labtech) after 1 hour.
443

β-arrestin recruitment assay. The LgBit-CAAX and β-arrestin1-SmBit plasmids were a gift from Sudar Rajagopal (Duke University). Inducible Expi293 cells were co-transfected with LgBit-CAAX, β-arrestin2-SmBit, and pcDNA-Zeo-tetO-Flag-AT1R[24] in a 1:4:5 ratio. Cells were induced 2 days post-transfection as described above. Three days post-transfection, cells were harvested and resuspended in Hanks' balanced salt solution + 20 mM HEPES pH 7.4 (assay buffer) containing Coelenterazine H (Research Products International) (3.1 μM), and 80 μL of cells were dispensed into opaque white 96-well plates. After reading basal luminescence 3 times (Clariostar, BMG LabTech), cells were treated with 20 μL of a serial dilution of ligands prepared in assay buffer containing 0.1% BSA. Luminescence values collected 20 minutes post-stimulation were normalized to the average of the three basal luminescence reads from the same well. A 3-parameter dose-response curve was fit to the normalized data from 3 independent experiments (GraphPad Prism).

Preparation of model for MD simulations. An X-ray crystal structure of the AT1R in the inactive conformation (PDB: 4YAY) was used as a starting structure for the MD simulations[29]. The co-crystallized small-molecule antagonist ZD7155 and the soluble cytochrome b562 were removed. The missing regions of the ECL2 and ICL3 were reconstructed using AlphaFold2[59]. The refined protein structure was aligned to the TM1, 2 and 4 helices of the entry 4YAY from the Orientation of Proteins in Membranes (OPM) database[60]. Next, TRV026 was placed into the orthosteric ligand binding pocket of the reconstructed inactive conformation using the ligand conformation and orientation from the TRV026-bound active AT1R structure (PDB: 6OS2)[26]. The simulation box of the system including water molecules, ions, lipids, and the TRV026-bound AT1R was built using CHARMM-GUI[61]. All residues were kept in the standard protonation states of the CHARMM36m force field, except D74$^{2.50}$ and D125$^{3.49}$, which were set as protonated. AT1R, in contrast to many class A GPCR representatives, does not have a sodium-binding site in proximity to D74$^{2.50}$, and, in the absence of sodium, D74$^{2.50}$ is likely to be protonated[30]. D125$^{3.49}$ is normally deprotonated in the inactive conformation and protonated in the active conformation; thus we set D125 as protonated in order to drive our simulation away from the inactive conformation[9]. The ligand-bound receptor was oriented in the membrane with the "Use PDB Orientation" option of the CHARMM-GUI. The number of POPC lipids in each upper- and lower leaflet was defined as 75. Na^+ and Cl^- ions were added to neutralize the net charge and reach physiological ionic strength, 0.15 M. The resulting output files with coordinates, topology, atom indexes, and parameters of the CHARMM36m force field were downloaded, and force field parameters for the non-standard residue Sar1 of TRV026 were adopted from the earlier publication[30]. The resulting system contained 70,200 atoms, 14,902 TIP3 water molecules, 150 POPC lipids, 39 Na^+ and 58 Cl^- ions. The rectangular simulation box was 79.062 x 79.062 x 12.082 Å.

MD simulations. We performed five independent replicas of unbiased molecular dynamics (MD) simulations using GROMACS, version 2021.3[62]. Each starting system was first subjected to energy minimization using 10,000 steps of the steepest descent algorithm. During minimization, both positional (POSRE) and dihedral (DIHRES) restraints were applied with the following force constants (in kJ mol^1 nm^2 for POSRE and kJ mol^1 rad^2 for DIHRES):

POSRE backbone	4000.0
POSRE side chains	2000.0
POSRE lipids	1000.0
DIHRES	1000.0

The equilibration phase consisted of six sequential steps. The first was a 125 ps NVT equilibration using the same force constants as during energy minimization. The second step was also 125 ps of NVT equilibration but with the reduced values of force constants (see table below). All

equilibration simulations were conducted at a target temperature of 303.15 K using the Berendsen thermostat[63]. The following four steps were NPT equilibration simulations: 125 ps in the third step, 500 ps in fourth step, 20,000 ps in fifth step, and 500 ps in sixth step. The restraint strengths were progressively reduced across the steps as follows:

	step 2	step 3	step 4	step 5	step 6
POSRE backbone	2000.0	1000.0	500.0	200.0	50.0
POSRE side chains	1000.0	500.0	200.0	50.0	0.0
POSRE lipids	400.0	400.0	200.0	40.0	0.0
DIHRES	400.0	200.0	200.0	100.0	0.0

During equilibration, pressure was controlled using a semi-isotropic Berendsen barostat, with the xy-plane and z-axis coupled independently[63]. A time step of 1 fs was used for equilibration steps 1–3, and 2 fs for steps 4–6. The overall equilibration time was 21,250 ps.

Each replica was followed by a 20 μs production MD simulation, carried out without any positional or dihedral constraints. Temperature and pressure were maintained using the velocity-rescale thermostat and the semi-isotropic Parrinello–Rahman barostat, respectively[64,65]. Long-range electrostatics were handled using the Particle Mesh Ewald (PME) method, with fourth-order interpolation and a real-space cut-off of 1.2 nm[66,67]. Van der Waals interactions were switched off smoothly between 1.0 and 1.2 nm. All covalent bonds involving hydrogen atoms were constrained to their equilibrium lengths using P-LINCS[68]. A 2 fs integration time step was used during production, with Verlet neighbor lists updated every 20 fs and the neighbor list radius set automatically.

Preparation of MD trajectory for analysis. For the analysis, we reconstructed periodic boundary conditions (PBC) using "gmx trjconv" command to ensure that the entire molecular system remained within a single unit cell without broken covalent bonds due to periodicity. We then applied procedures of rotation and translation to align AT1R to its starting structure using "gmx trjconv". The alignment was performed on the backbone heavy atoms of TM1, TM2, and TM4, since these helices are known to remain relatively rigid across different conformational states of GPCRs[69,70]. This selection of atoms for alignment allowed us to minimize alignment artifacts. This postprocessing protocol eliminated the need for additional alignment steps in subsequent analyses and enabled more straightforward visual inspection of the trajectories using PyMOL.

To reduce computational complexity for downstream analyses, we generated a shortened version of the 20 μs-long post-processed MD trajectory. This reduced dataset consisted of 2000 frames, extracted at 10 ns intervals.

Measurement of TM1–TM6 distance. In this study, the "TM1–TM6" distance refers to the distance between the Cα atoms of residues $F55^{1.59}$ and $D236^{6.31}$. We calculated this distance along the MD trajectory using the MDanalysis Python package[71,72]. We plotted changes of the TM1–TM6 distance across the time-trace as a semi-transparent line **(Figure 5A)**, with a bold line of a sliding mean.

Simulation of DEER distance distributions for an MD trajectory. To simulate DEER distance distributions, we used the chiLife Python package[73]. Typically, chiLife works with single structures loaded into a Universe object. Since the Universe object is a feature of the MDAnalysis, we utilized this library to load the entire MD trajectory into the Universe object. This enabled us to iterate through the MD simulation frames and simulate DEER distance distributions for each frame individually.

546
547 For our analysis, we used the V1 spin label, consistent with that used in the corresponding DEER
548 experiments[9]. The labeling positions are shown in **Figure 2A**. At each labeling site, ensembles
549 of V1 spin label conformers were generated using the Accessible Volume (AV) approach, with 10
550 000 iterations[73].
551
552 *Calculation of RMSF.* We computed Root Mean Square Fluctuation (RMSF) for all Cα atoms of
553 AT1R. To do this, we used MD simulation frames recorded after 5 μs, as these represented the
554 intermediate structure.
555
556 The RMSF values were added to the B-factor column of the .pdb file with the representative
557 intermediate structure. To illustrate flexibility of different segments of AT1R, we visualized the
558 obtained RMSF values as a putty plot **(Figure 5B)**, using PyMOL version 2.5 Schrödinger, LLC[74].
559
560 *Alignment of the model with GPCR-arrestin complexes.* To investigate why arrestin binding to
561 TRV026-bound AT1R may be hindered, we aligned GPCR–arrestin complexes from the PDB to
562 the structural model of the intermediate conformation. All downloaded GPCR–arrestin complexes
563 were aligned in PyMol using the backbone heavy atoms. The PDB identifiers of the GPCR–
564 arrestin complexes used in the alignment are listed in **Supplementary Table 4**.

565 **References**

566 1. Karnik, S.S. et al. International Union of Basic and Clinical Pharmacology. XCIX.
567 Angiotensin Receptors: Interpreters of Pathophysiological Angiotensinergic Stimuli
568 [corrected]. *Pharmacol Rev* **67**, 754-819 (2015).
569 2. Liu, S., Anderson, P.J., Rajagopal, S., Lefkowitz, R.J. & Rockman, H.A. G Protein-
570 Coupled Receptors: A Century of Research and Discovery. *Circ Res* **135**, 174-197
571 (2024).
572 3. Abraham, D.M. et al. beta-Arrestin mediates the Frank-Starling mechanism of cardiac
573 contractility. *Proc Natl Acad Sci U S A* **113**, 14426-14431 (2016).
574 4. Kim, K.S. et al. beta-Arrestin-biased AT1R stimulation promotes cell survival during
575 acute cardiac injury. *Am J Physiol Heart Circ Physiol* **303**, H1001-10 (2012).
576 5. Cotter, G. et al. Relationship between baseline systolic blood pressure and long-term
577 outcomes in acute heart failure patients treated with TRV027: an exploratory subgroup
578 analysis of BLAST-AHF. *Clin Res Cardiol* **107**, 170-181 (2018).
579 6. Pang, P.S. et al. Biased ligand of the angiotensin II type 1 receptor in patients with acute
580 heart failure: a randomized, double-blind, placebo-controlled, phase IIB, dose ranging
581 trial (BLAST-AHF). *Eur Heart J* **38**, 2364-2373 (2017).
582 7. Robbins, A.J. et al. The effect of TRV027 on coagulation in COVID-19: A pilot
583 randomized, placebo-controlled trial. *Br J Pharmacol* **89**, 1495-1501 (2023).
584 8. Self, W.H. et al. Renin-Angiotensin System Modulation With Synthetic Angiotensin (1-7)
585 and Angiotensin II Type 1 Receptor-Biased Ligand in Adults With COVID-19: Two
586 Randomized Clinical Trials. *JAMA* **329**, 1170-1182 (2023).
587 9. Wingler, L.M. et al. Angiotensin Analogs with Divergent Bias Stabilize Distinct Receptor
588 Conformations. *Cell* **176**, 468-478 e11 (2019).
589 10. Elgeti, M. & Hubbell, W.L. DEER Analysis of GPCR Conformational Heterogeneity.
590 *Biomolecules* **11**, 778 (2021).
591 11. Gurevich, V.V. & Benovic, J.L. Visual arrestin interaction with rhodopsin. Sequential
592 multisite binding ensures strict selectivity toward light-activated phosphorylated
593 rhodopsin. *J Biol Chem* **268**, 11628-38 (1993).
594 12. Gurevich, V.V., Gurevich, E.V. & Uversky, V.N. Arrestins: structural disorder creates rich
595 functionality. *Protein Cell* **9**, 986-1003 (2018).
596 13. Gurevich, V.V., Pals-Rylaarsdam, R., Benovic, J.L., Hosey, M.M. & Onorato, J.J.
597 Agonist-receptor-arrestin, an alternative ternary complex with high agonist affinity. *J Biol*
598 *Chem* **272**, 28849-52 (1997).
599 14. Chen, K. et al. Tail engagement of arrestin at the glucagon receptor. *Nature* **620**, 904-
600 910 (2023).
601 15. Staus, D.P. et al. Structure of the M2 muscarinic receptor-beta-arrestin complex in a lipid
602 nanodisc. *Nature* **579**, 297-302 (2020).
603 16. Huang, W. et al. Structure of the neurotensin receptor 1 in complex with beta-arrestin 1.
604 *Nature* **579**, 303-308 (2020).
605 17. Chen, Q. et al. Effect of phosphorylation barcodes on arrestin binding to a chemokine
606 receptor. *Nature* (2025).
607 18. Shukla, A.K. et al. Visualization of arrestin recruitment by a G-protein-coupled receptor.
608 *Nature* **512**, 218-222 (2014).
609 19. Cahill, T.J., 3rd et al. Distinct conformations of GPCR-beta-arrestin complexes mediate
610 desensitization, signaling, and endocytosis. *Proc Natl Acad Sci U S A* **114**, 2562-2567
611 (2017).
612 20. Kumari, P. et al. Functional competence of a partially engaged GPCR-beta-arrestin
613 complex. *Nat Commun* **7**, 13416 (2016).
614 21. Shukla, A.K. et al. Structure of active beta-arrestin-1 bound to a G-protein-coupled
615 receptor phosphopeptide. *Nature* **497**, 137-41 (2013).

616 22. Xiao, K., Shenoy, S.K., Nobles, K. & Lefkowitz, R.J. Activation-dependent
617 conformational changes in beta-arrestin 2. *J Biol Chem* **279**, 55744-53 (2004).
618 23. Zhang, D. et al. Structural insights into angiotensin receptor signaling modulation by
619 balanced and biased agonists. *EMBO J* **42**, e112940 (2023).
620 24. Wingler, L.M., McMahon, C., Staus, D.P., Lefkowitz, R.J. & Kruse, A.C. Distinctive
621 Activation Mechanism for Angiotensin Receptor Revealed by a Synthetic Nanobody. *Cell*
622 **176**, 479-490 e12 (2019).
623 25. Van Eps, N. et al. Conformational equilibria of light-activated rhodopsin in nanodiscs.
624 *Proc Natl Acad Sci U S A* **114**, E3268-E3275 (2017).
625 26. Wingler, L.M. et al. Angiotensin and biased analogs induce structurally distinct active
626 conformations within a GPCR. *Science* **367**, 888-892 (2020).
627 27. Violin, J.D. et al. Selectively engaging beta-arrestins at the angiotensin II type 1 receptor
628 reduces blood pressure and increases cardiac performance. *J Pharmacol Exp Ther* **335**,
629 572-9 (2010).
630 28. Dror, R.O. et al. Activation mechanism of the beta2-adrenergic receptor. *Proc Natl Acad*
631 *Sci U S A* **108**, 18684-9 (2011).
632 29. Zhang, H. et al. Structure of the Angiotensin receptor revealed by serial femtosecond
633 crystallography. *Cell* **161**, 833-44 (2015).
634 30. Suomivuori, C.M. et al. Molecular mechanism of biased signaling in a prototypical G
635 protein-coupled receptor. *Science* **367**, 881-887 (2020).
636 31. Zhang, H. et al. Structural basis for selectivity and diversity in angiotensin II receptors.
637 *Nature* **544**, 327-332 (2017).
638 32. Chen, Q. & Tesmer, J.J.G. G protein-coupled receptor interactions with arrestins and
639 GPCR kinases: The unresolved issue of signal bias. *J Biol Chem* **298**, 102279 (2022).
640 33. Staus, D.P., Wingler, L.M., Pichugin, D., Prosser, R.S. & Lefkowitz, R.J. Detergent- and
641 phospholipid-based reconstitution systems have differential effects on constitutive
642 activity of G-protein-coupled receptors. *J Biol Chem* **294**, 13218-13223 (2019).
643 34. Lally, C.C., Bauer, B., Selent, J. & Sommer, M.E. C-edge loops of arrestin function as a
644 membrane anchor. *Nat Commun* **8**, 14258 (2017).
645 35. Grimes, J. et al. Plasma membrane preassociation drives beta-arrestin coupling to
646 receptors and activation. *Cell*, 2238-2255.e20 (2023).
647 36. Latorraca, N.R. et al. How GPCR Phosphorylation Patterns Orchestrate Arrestin-
648 Mediated Signaling. *Cell* **183**, 1813-1825 e18 (2020).
649 37. Maharana, J. et al. Structural snapshots uncover a key phosphorylation motif in GPCRs
650 driving beta-arrestin activation. *Mol Cell*, 2091-2107.e7 (2023).
651 38. Cao, C. et al. Signaling snapshots of a serotonin receptor activated by the prototypical
652 psychedelic LSD. *Neuron* **110**, 3154-3167 e7 (2022).
653 39. Lee, Y. et al. Molecular basis of beta-arrestin coupling to formoterol-bound beta(1)-
654 adrenoceptor. *Nature* **583**, 862-866 (2020).
655 40. Bous, J. et al. Structure of the vasopressin hormone-V2 receptor-beta-arrestin1 ternary
656 complex. *Sci Adv* **8**, eabo7761 (2022).
657 41. Yin, W. et al. A complex structure of arrestin-2 bound to a G protein-coupled receptor.
658 *Cell Res* **29**, 971-983 (2019).
659 42. Kang, Y. et al. Crystal structure of rhodopsin bound to arrestin by femtosecond X-ray
660 laser. *Nature* **523**, 561-7 (2015).
661 43. Bumbak, F. et al. Stabilization of pre-existing neurotensin receptor conformational states
662 by beta-arrestin-1 and the biased allosteric modulator ML314. *Nat Commun* **14**, 3328
663 (2023).
664 44. Xu, J. et al. Structural and dynamic insights into supra-physiological activation and
665 allosteric modulation of a muscarinic acetylcholine receptor. *Nat Commun* **14**, 376
666 (2023).

45. Seyedabadi, M., Gharghabi, M., Gurevich, E.V. & Gurevich, V.V. Structural basis of GPCR coupling to distinct signal transducers: implications for biased signaling. *Trends Biochem Sci* **47**, 570-581 (2022).
46. Staus, D.P. et al. Sortase ligation enables homogeneous GPCR phosphorylation to reveal diversity in beta-arrestin coupling. *Proc Natl Acad Sci U S A* **115**, 3834-3839 (2018).
47. Kawakami, K. et al. Heterotrimeric Gq proteins act as a switch for GRK5/6 selectivity underlying beta-arrestin transducer bias. *Nat Commun* **13**, 487 (2022).
48. Drube, J. et al. GPCR kinase knockout cells reveal the impact of individual GRKs on arrestin binding and GPCR regulation. *Nat Commun* **13**, 540 (2022).
49. Wei, H., Ahn, S., Barnes, W.G. & Lefkowitz, R.J. Stable interaction between beta-arrestin 2 and angiotensin type 1A receptor is required for beta-arrestin 2-mediated activation of extracellular signal-regulated kinases 1 and 2. *J Biol Chem* **279**, 48255-61 (2004).
50. Matthees, E.S.F. et al. Relating GPCR domains with functionality: receptor helix-bundle and C-terminus differentially influence GRK-specific functions and β-arrestin-mediated regulation. *bioRxiv*, 2024.09.30.615794 (2024).
51. Zimmerman, B. et al. Differential beta-arrestin-dependent conformational signaling and cellular responses revealed by angiotensin analogs. *Sci Signal* **5**, ra33 (2012).
52. Santos, G.A. et al. Comparative analyses of downstream signal transduction targets modulated after activation of the AT1 receptor by two beta-arrestin-biased agonists. *Front Pharmacol* **6**, 131 (2015).
53. Liu, Q. et al. DeSiphering receptor core-induced and ligand-dependent conformational changes in arrestin via genetic encoded trimethylsilyl (1)H-NMR probe. *Nat Commun* **11**, 4857 (2020).
54. Petrovic, I. et al. Arrestin recognizes GPCRs independently of the receptor state. *Proc Natl Acad Sci U S A* **122**, e2501487122 (2025).
55. Xu, J. et al. Conformational Complexity and Dynamics in a Muscarinic Receptor Revealed by NMR Spectroscopy. *Mol Cell* **75**, 53-65 e7 (2019).
56. Staus, D.P. et al. Allosteric nanobodies reveal the dynamic range and diverse mechanisms of G-protein-coupled receptor activation. *Nature* **535**, 448-52 (2016).
57. Pannier, M., Veit, S., Godt, A., Jeschke, G. & Spiess, H.W. Dead-time free measurement of dipole-dipole interactions between electron spins. *J Magn Reson* **142**, 331-40 (2000).
58. Altenbach, C. LongDistances—a program to analyze DEER data. *EPR Newsletter* **31**, 12-13 (2021).
59. Jumper, J. & Hassabis, D. Protein structure predictions to atomic accuracy with AlphaFold. *Nat Methods* **19**, 11-12 (2022).
60. Lomize, M.A., Pogozheva, I.D., Joo, H., Mosberg, H.I. & Lomize, A.L. OPM database and PPM web server: resources for positioning of proteins in membranes. *Nucleic Acids Res* **40**, D370-6 (2012).
61. Jo, S., Kim, T., Iyer, V.G. & Im, W. CHARMM-GUI: a web-based graphical user interface for CHARMM. *J Comput Chem* **29**, 1859-65 (2008).
62. Van Der Spoel, D. et al. GROMACS: fast, flexible, and free. *J Comput Chem* **26**, 1701-18 (2005).
63. Berendsen, H.J.C., Postma, J.P.M., Vangunsteren, W.F., Dinola, A. & Haak, J.R. Molecular-Dynamics with Coupling to an External Bath. *J Chem Phys* **81**, 3684-3690 (1984).
64. Parrinello, M. & Rahman, A. Polymorphic Transitions in Single-Crystals - a New Molecular-Dynamics Method. *J Appl Phys* **52**, 7182-7190 (1981).
65. Bussi, G., Donadio, D. & Parrinello, M. Canonical sampling through velocity rescaling. *J Chem Phys* **126**, 014101 (2007).

66. Darden, T., York, D. & Pedersen, L. Particle Mesh Ewald - an N.Log(N) Method for Ewald Sums in Large Systems. *J Chem Phys* **98**, 10089-10092 (1993).
67. Essmann, U. et al. A Smooth Particle Mesh Ewald Method. *J Chem Phys* **103**, 8577-8593 (1995).
68. Hess, B. P-LINCS: A Parallel Linear Constraint Solver for Molecular Simulation. *J Chem Theory Comput* **4**, 116-22 (2008).
69. Weis, W.I. & Kobilka, B.K. The Molecular Basis of G Protein-Coupled Receptor Activation. *Annu Rev Biochem* **87**, 897-919 (2018).
70. Dalton, J.A., Lans, I. & Giraldo, J. Quantifying conformational changes in GPCRs: glimpse of a common functional mechanism. *BMC Bioinformatics* **16**, 124 (2015).
71. Gowers, R.J. et al. MDAnalysis: A Python Package for the Rapid Analysis of Molecular Dynamics Simulations. in *Proceedings of the 15th Python in Science Conference* (eds Benthall, S. & Rostrup, S.) 98-105 (SciPy, Austin, TX, 2016).
72. Michaud-Agrawal, N., Denning, E.J., Woolf, T.B. & Beckstein, O. MDAnalysis: a toolkit for the analysis of molecular dynamics simulations. *J Comput Chem* **32**, 2319-27 (2011).
73. Tessmer, M.H. & Stoll, S. chiLife: An open-source Python package for in silico spin labeling and integrative protein modeling. *PLoS Comput Biol* **19**, e1010834 (2023).
74. Elgeti, M. et al. Precision vs flexibility in GPCR signaling. *J Am Chem Soc* **135**, 12305-12 (2013).

ACKNOWLEDGEMENTS

We thank Robert J. Lefkowitz for critical reading of this manuscript. We thank Wayne L. Hubbell for the use of his equipment for DEER experiments. The authors gratefully acknowledge the computing time provided by them on the high-performance computers Barnard and Romeo at NHR@TUD, which is funded by the Federal Ministry of Education and Research and the state governments participating on the basis of the resolutions of the GWK for the national high-performance computing at universities (www.nhr-verein.de/unsere-partner). This work was funded by the German Federal Ministry of Education and Research, SECAI 57616814 to J.B., and the German Research Foundation, project number 421152132, subproject A03 and project number 514664767, subproject B07 to M.E. L.M.W. is a Whitehead Scholar and a Pew Scholar in the Biomedical Sciences, supported by The Pew Charitable Trusts.

CONTRIBUTIONS

M.E. and L.M.W. conceived the study. D.P.S. contributed new reagents and protocols. L.M.W. purified proteins, prepared DEER samples, and performed *in vitro* biochemical experiments, radioligand binding, and cellular assays. M.E. performed DEER experiments and data analysis. M.B.H. and J.B. performed and analyzed MD simulations. J.B., M.E., and L.M.W. wrote the manuscript.

COMPETING INTERESTS

L.M.W. is a scientific advisor for Septerna, Inc. D.P.S. is an employee of Septerna, Inc.